LITHOS 406–407 (2021) 106507

Contents lists available at ScienceDirect

LITHOS

journal homepage: www.elsevier.com/locate/lithos

# New geochemical and geochronological data on the Cenozoic Veneto Volcanic Province: Geodynamic inferences

V. Brombin [a,b], E.A. Pettitt [c], M.F. Fahnestock [c], M. Casalini [d], L.E. Webb [e], J.G. Bryce [c], G. Bianchini [a,b,*]

[a] Department of Physics and Earth Sciences, University of Ferrara, Via G. Saragat 1, 44122 Ferrara, Italy
[b] Institute of Environmental Geology and Geoengineering of the Italian National Research Council (CNR-IGAG), Rome, Italy
[c] Department of Earth Science, University of New Hampshire, Durham, NH 03824, USA
[d] Department of Earth Sciences, University of Florence, Via G. La Pira 4, 50121 Florence, Italy
[e] Department of Geology, University of Vermont, Burlington, VT 05405, USA

ARTICLE INFO

*Keywords:*
Veneto Volcanic Province
Intraplate magmatism
$^{40}Ar/^{39}Ar$ and K/Ar geochronology
Giudicarie Fault System
Poloidal mantle flow

ABSTRACT

The Veneto Volcanic Province (VVP; NE Italy) is an intraplate magmatic area whose activity occurred intermittently in the Cenozoic, generating five districts (Val d'Adige, Lessini Mts., Marostica Hills, Berici Hills, and Euganean Hills). This intraplate magmatism was concomitant to the collision of the European plate and Adria microplate and the orogenesis of the neighboring Alpine belt. Different geodynamic models suggested relationships between VVP and the coexisting subduction processes. To give new insights on this on-going debate, this work provides new petrographic and geochemical data, including Sr-Nd-Pb isotopic and $^{40}Ar/^{39}Ar$ and K—Ar geochronological analyses for lavas sampled in the Lessini Mts. and Val d'Adige, which are the oldest VVP magmatic districts, as well as Marostica Hills and Berici Hills, which are the least investigated districts. The trace element distribution indicates that VVP melts were variously affected by metasomatic enrichments stabilized as phlogopite and/or amphibole. The Sr-Nd-Pb isotope ratios conform to the dominant features of sub-lithospheric mantle components widespread at regional scale throughout the whole European and Mediterranean area. Within this framework, the geochronological data indicate that the oldest magmatic episodes occurred in the Eocene (45–42 Ma) in the Lessini Mts. and Val d'Adige, simultaneously with the orogenic magmatism of Adamello intrusive complex along the Giudicarie Fault, a portion of the Periadriatic lineament which is an important Alpine suture. In our geodynamic reconstruction we propose that the Giudicarie Fault is the superficial expression of a slab tear, responsible for the uprising of an asthenospheric poloidal mantle flow, which induced both the Adamello and VVP magmatism. Subsequently, VVP activity migrated eastwards following the general mantle flow as indicated by minor volcanic pulses in the Euganean and Marostica Hills during Oligocene and Miocene.

## 1. Introduction

The Paleogene convergence of the European plate with the Adria microplate led to the formation of the Alpine belt (Handy et al., 2010, 2015; Wiederkehr et al., 2009) and the occurrence of Cenozoic orogenic (subduction-related) and anorogenic (intraplate-like) magmatic activities along the Periadriatic line and in the Southeastern Alpine domain, respectively (Fig. 1a, b; Beccaluva et al., 2007; Bellieni et al., 2010; Bergomi et al., 2015; Brack, 1984; Brombin et al., 2019; Callegari and Brack, 2002; Conticelli et al., 2009; Ji et al., 2019; Kagami et al., 1991; Macera et al., 2003, 2008; Schaltegger et al., 2019). In the mid-Nineties, the occurrence of *syn*- and post-collisional magmatism along the Periadriatic line was investigated by Davies and von Blanckenburg (1995), which introduced for the first time the slab breakoff model. According to this theory, the Periadriatic magmatism near the subduction zone is the effect of mantle upwelling through a slab window, after the slab breakoff of the subducting European plate, which probably occurred ~35 Ma (Dézes et al., 2004; Rosenbaum and Lister, 2005; Stampfli et al., 1998, 2002). The same geodynamic interpretation was also applied to explain the occurrence of intraplate-like magmatism in the Southeastern Alpine

* Corresponding author at: Department of Physics and Earth Sciences, University of Ferrara, Via G. Saragat 1, 44122 Ferrara, Italy.
*E-mail address:* bncglc@unife.it (G. Bianchini).

https://doi.org/10.1016/j.lithos.2021.106507
Received 7 April 2021; Received in revised form 18 October 2021; Accepted 18 October 2021
Available online 22 October 2021

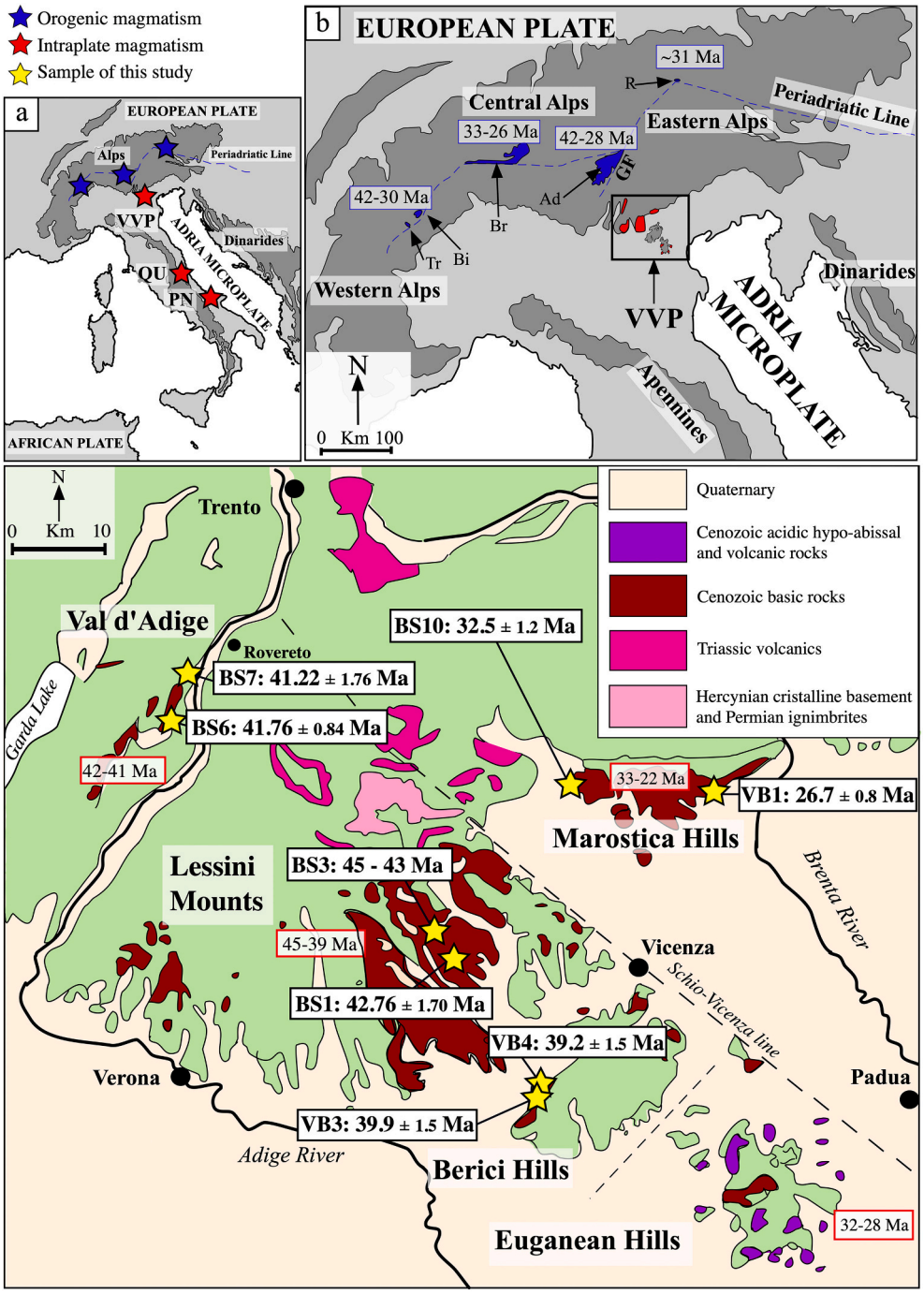


**Fig. 1.** Simplified geological map of the Veneto Volcanic Province (VVP), showing the locations of the samples collected for this work and the obtained ages (see Section 4.3). The new ages are framed with black lines, whereas literature ages are framed with red lines (from Brombin et al., 2019 and references therein). Inset (a) location of the VVP in the Italian peninsula, general view of the major lithospheric plates involved in the area, and distribution of other Cenozoic volcanic occurrences in the Adria microplate having intraplate c affinity. Abbreviations: QU: Mount Queglia; PN: Pietre Nere. Inset (b) VVP spatial distribution in relation to the surrounding orogenic belts with locations of Periadriatic intrusive bodies along the Periadriatic line and the relative intrusive rock ages (from Kästle et al., 2020 and reference therein). Abbreviations: Tr: Traversella; Bi: Biella; Br: Bregaglia; Ad: Adamello; R = Rensen. (For interpretation of the references to colour in this figure legend, the reader is referred to the web version of this article.)

domain, which generated the Veneto Volcanic Province (VVP; De Vecchi and Sedea, 1995; Fig. 1), *i.e.*, one of the largest Cenozoic magmatic districts of the Adria Plate. Macera et al. (2003) proposed that the VVP was related to mantle diapirs, which were sucked into the European slab window and upwelled toward shallower levels heating the overriding Adria plate, triggering partial melting, and finally, inducing the VVP magmatism. However, recent high-resolution tomographic images displayed an unbroken subvertical European slab (Hua et al., 2017; Salimbeni et al., 2018; Zhao et al., 2016). In the absence of robust evidence for slab breakoff, several authors proposed alternative geodynamic interpretations for the occurrence of the Cenozoic magmatism in the Alpine domain. Such interpretations have been formulated mainly investigating new geochronological data in order to reconstruct the temporal evolution of the magmatic activities in the Alpine domain. Interestingly, the geochronological studies also indicated that the magmatic activities in the Alpine domain began before the supposed slab breakoff (*i.e.*, ~35 Ma). Using zircon U—Pb ages from the main Periadriatic intrusives of the Western (Traversella and Biella) and Central (Bregaglia and Adamello) Alps, Ji et al. (2019) demonstrated that several magmatic events started synchronously along the Periadriatic line since the middle Eocene (~45 Ma) and proposed that the Periadriatic magmatism was triggered by a mantle corner flow, induced by the progressive European slab steepening. Brombin et al. (2019) reconstructed the intraplate magmatic activity of the VVP from the Eocene to early Miocene, on the basis of new $^{40}Ar/^{39}Ar$ ages of VVP magmatic products. These authors invoked the upwelling of a poloidal mantle flow, overpassing the front edge of the steeping slab to explain the occurrence of VVP magmatic activities. However, considering that

the beginning of the VVP magmatic activity is not well defined, new geochemical, isotopic, and geochronological analyses are necessary to understand the onset of the VVP volcanism within the Alpine tectono-magmatic framework. Here, we present these data and then interpret them to provide a new geodynamic explanation for the spatial-temporal contiguity of the intraplate basic magmatic products typical of the VVP and the orogenic magmas outcropping northward along the Periadriatic fault system that is one of the main tectonic discontinuities of the entire Alpine belt. In this light, this work contributes to recognize the deep features of the Alpine geodynamic architecture.

## 2. Geological overview

During the Cenozoic, the Southeastern Alpine domain was affected by effusive to subvolcanic magmatic activity, mainly basic-ultrabasic in composition, that took place intermittently from the late Paleocene to the early Miocene (Bassi et al., 2008; Beccaluva et al., 2007; Brombin et al., 2019; De Vecchi and Sedea, 1995; Macera et al., 2003). Most of the magmatic products crop out intermittently over a NNW-SSE elongated area of about 1500 km$^2$ and formed five main VVP magmatic districts: Val d'Adige, Lessini Mts., Marostica Hills, Berici Hills, and Euganean Hills (Beccaluva et al., 2007) (Fig. 1). According to the temporal reconstruction of VVP magmatic activities reported in the literature (Brombin et al., 2019, and reference therein), the first magmatic events occurred during the Paleocene-Eocene in the westernmost districts (Val d'Adige and Lessini Mts.), and only in the Oligocene-Miocene in the easternmost districts (Berici Hills, Euganean Hills, and Marostica Hills). However, the onset of the magmatism, generally ascribed to the Paleocene, is questionable as the age was inferred only by stratigraphic evidence of submarine volcanic products described in past studies (Barbieri, 1972; Medizza, 1965). The oldest radioisotopic age recorded in the VVP is ~51 Ma (Eocene), which results from some zircons hosted in a basanite of the Lessini Mts. analyzed by Visonà et al. (2007). This dating is discarded in this work, as the relative data are not concordant and the zircons were not crystallized directly from the erupted magma (see Brombin et al., 2019 for a review).

From the petrographic and petrological point of view, VVP magmatic products are basalts *sensu lato* ($SiO_2$ < 55 wt%, MgO >6 wt%; Wilson and Downes, 2006), ranging in composition from highly alkaline products that are strongly silica under-saturated (nephelinites) to alkaline (basanites and alkaline basalts) and subalkaline (tholeiitic basalts) magmatic products (Beccaluva et al., 2007; Macera et al., 2003). Only in the Euganean Hills, more differentiated magmatic products, such as rhyolites, trachytes, and subordinate latites are also present (Milani et al., 1999). Previous studies link VVP petrological and geochronological data to the geodynamic framework, but key age constraints are lacking to establish a clear causal link between the timing of volcanism and the nature of the related magmas with the tectonic processes occurring at a regional scale.

## 3. Material and methods

### 3.1. Sampling

For this study, four samples were collected in the Lessini Mts. and Val d'Adige districts (Fig. 1), *i.e.*, the westernmost and plausibly oldest VVP occurrences (Brombin et al., 2019 and reference therein). In particular, two samples were collected from the central portion of Lessini Mts.: BS1 was collected in a quarry of columnar basalts in the town of San Giovanni Ilarione and BS3 in a lava flow near the famous Bolca Fossil-Lagerstätte area (Papazzoni et al., 2014, and references therein). Two samples were collected from Val d'Adige: BS6 was sampled in a basaltic lava flow of the Northeastern part of Monte Baldo and BS7 in a volcanic neck near the town of Rovereto. Other four samples were also collected South- and East-ward in the Marostica Hills and Berici Hills (Fig. 1), as these districts are still scarcely investigated and poorly constrained in age. For Marostica Hills, two samples were collected: BS10 is from the western border of the district and VB1 is from the volcanic neck of Monte Gloso, which cut the middle Oligocene marine sediments. In the Berici Hills, almost all the magmatic products are covered by the overlain marine sediments, and the two samples of this study (VB3 and VB4) were collected from intruded sills in the Southwestern edge of this district.

### 3.2. Analytical methods

After removal of visibly weathered material, samples were cut for the preparation of thin sections that were investigated with an optical microscope. For each sample, the proportions of phenocrysts and matrix (*i.e.*, microlites and glass) were determined by point counting on thin section (~1000 point per sample). The samples were analyzed for the major-element compositions of minerals using a CAMECA SX 50 electron microprobe (EMP) at the CNR "Istituto di Geologia Ambientale e Geoingegneria" laboratories of the University of Rome "La Sapienza" (Italy). Analytical conditions were as follows: 15 kV acceleration potential; beam size focused at 5 μm; 15 nA beam current; 20–30 s counting time, as a function of the analyzed element. Silicate minerals and synthetic oxides were employed as standards.

Other sample aliquots were crushed, and fresh chips were powdered using an agate ring mill. Whole-rock major and trace elements of samples were determined by Wavelength Dispersive X-Ray Fluorescence Spectrometry (WDXRF) on pressed powder pellets at the Department of Physics and Earth Sciences, University of Ferrara (Italy), using an ARL Advant-XP spectrometer. Accuracy is estimated on the basis of repeated analyses of standards, generally lower than 2% for major oxides and less than 5% for trace element determinations, whereas the detection limits for trace elements range from 1 to 2 ppm (Supplementary Table 1a). Volatile contents were determined as loss on ignition (LOI) at 1000 °C.

For the determination of additional trace elements, sample powders were totally digested in PFA Savillex beakers with a mixture of HF and $HNO_3$. Dissolved samples were dried out and then re-dissolved in 2% $HNO_3$. The analyses were performed at the Department of Earth Sciences, University of Florence (Italy) with an Agilent 7800 ICP-MS using Rh as internal standard and a multi-elemental standard solution for calibration (Inorganic Ventures, VA, USA). Accuracy and precision, calculated on the base of repeated analyses of samples and rock standards (AGV-1, BHVO-1, BCR-2) were better than 10% for all the analyzed elements (Supplementary Table 1b).

The whole rock Sr and Nd isotopic compositions were determined at the Department of Earth Sciences, University of Florence. Sample powders were preliminarily leached with 1 N HCl (*e.g.*, for 1 h in an ultrasonic bath and rinsing with Milli-Q water) before the HF - $HNO_3$ - HCl acid digestion. Sr and Nd purification has been carried out using standard chromatographic techniques (*e.g.*, Avanzinelli et al., 2005). Sr and Nd isotopes were measured by magnetic sector multi-collector ThermoFisher Triton-Ti Plus mass spectrometer in static mode and the effect of mass fractionation has been corrected using an exponential law to $^{86}Sr/^{88}Sr = 0.1194$ and $^{146}Nd/^{144}Nd = 0.7219$, respectively. Repeated analyses of NIST SRM 987 and a Nd internal standard (Nd-Fi) yielded $^{87}Sr/^{86}Sr = 0.710256 \pm 5$ (2σ, $n = 3$), and $^{143}Nd/^{144}Nd = 0.511469 \pm 14$ (2σ, n = 3) over the period of analyses. The Nd isotope composition of the internal standard Nd-Fi is referred to the La Jolla $^{143}Nd/^{144}Nd = 0.511847 \pm 7$ (2σ, $n = 53$). These values are in well agreement with the long-term reproducibility of the laboratory and with reference values. Total procedural blanks were well below 100 pg, so negligible with respect to the sample size.

Given relatively homogenous major and trace elemental and Sr—Nd isotope compositions, Pb isotope characterization was restricted on a subset of samples (BS1, BS3, BS6, BS7, and BS10). The Pb isotope analyses were carried out at the Department of Earth Science of University of New Hampshire (USA). After powder sample digestion using a mixture of concentrated HF-$HNO_3$, Pb was collected using techniques

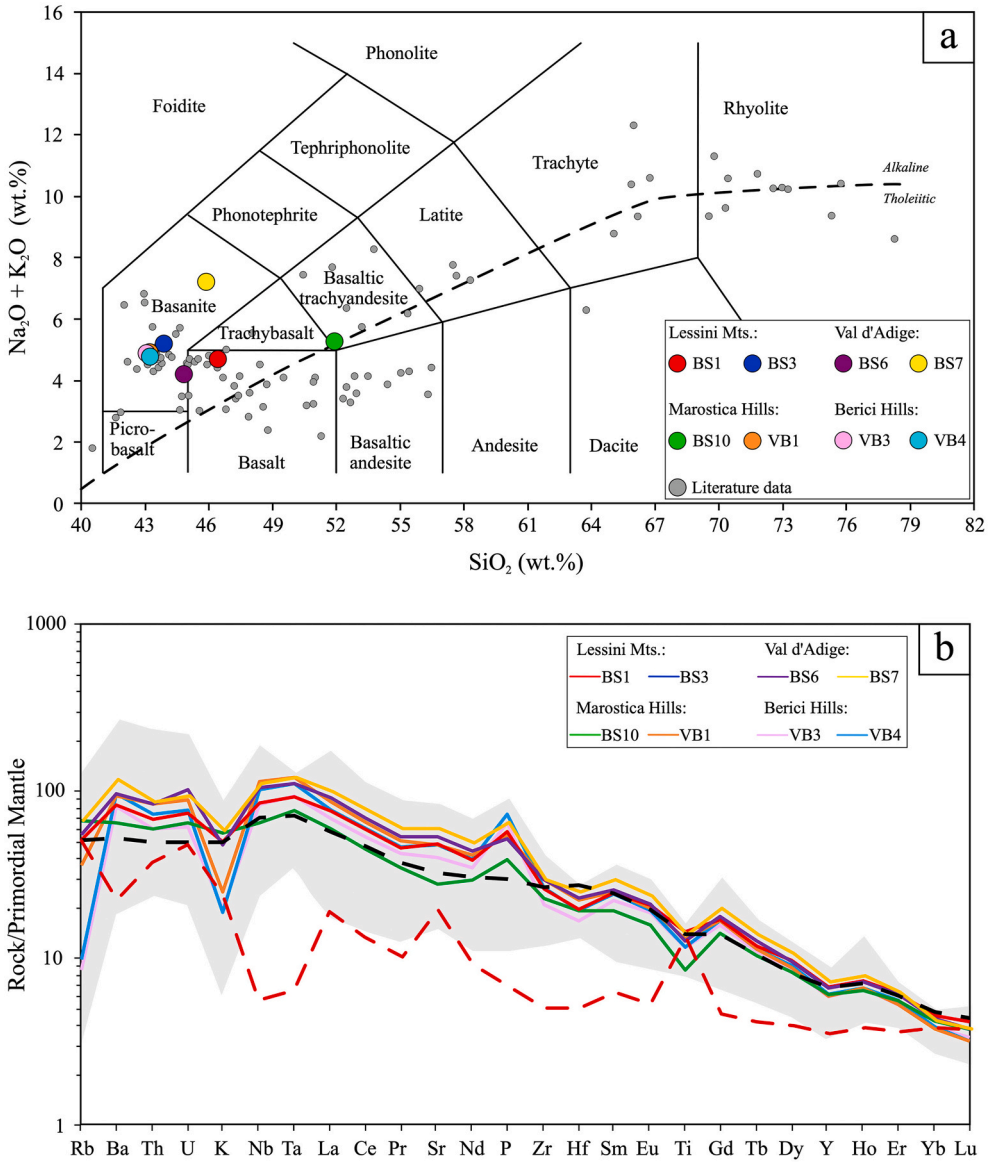


**Fig. 2.** a) Total Alkali *vs.* Silica (TAS) classification diagram (Le Maitre et al., 2002), reporting the composition of VVP samples studied in this work (large symbols) and that reported in the literature (small symbols; Beccaluva et al., 2007; Brombin et al., 2019; Macera et al., 2003; Milani et al., 1999). The alkaline-tholeiitic discrimination line is from Irvine and Baragar (1971). b) Primordial mantle-normalized (McDonough and Sun, 1995) incompatible trace element patterns of VVP samples studied in this paper, compared with those of other VVP products (shaded area) retrieved from the literature (Beccaluva et al., 2007; Brombin et al., 2019; Macera et al., 2003). The black dashed line is for Ocean Island Basalt composition (OIB; Sun and McDonough, 1989). The (average) trace element pattern of basic dykes from the Adamello plutonic complex (Hürlimann et al., 2016) is also reported for comparison.

adapted from Bryce and DePaolo (2004). Isotopic measurements were performed on a Nu Plasma II ES Multi-Collector Inductively Coupled Plasma Mass Spectrometer (MC-ICP-MS), following procedures outlined in Bianchini et al. (2014). Fourteen NIST SRM 981 aliquots were run as unknown samples, yielding averages (with 2σ) of $^{208}Pb/^{204}Pb = 36.7257 \pm 0.0053$, $^{207}Pb/^{204}Pb = 15.4975 \pm 0.0014$ and $^{206}Pb/^{204}Pb = 16.9407 \pm 0.0016$, all within in close agreement with the values reported by Eisele et al. (2003). Total procedural blanks were < 100 pg.

For geochronology both $^{40}Ar/^{39}Ar$ and K/Ar methods were employed. The $^{40}Ar/^{39}Ar$ plateau ages are preferable with respect to K/Ar ages because they are calculated by pooling the ages of several gas increments that can be cross checked. This type of analysis was specifically carried out on samples from the Val d'Adige and Lessini Mts., where previous studies identified the oldest VVP products, as we wanted to refine the information concerning the onset of the VVP magmatism that is still debated in the literature (see Brombin et al., 2019 for a review). Additional K/Ar analyses were carried out on samples from the Marostica and Berici Hills, just to verify if the spatial-temporal variation proposed by earlier papers is consistent. The geochronology analyses were performed using $^{40}Ar/^{39}Ar$ dating technique for samples BS1, BS3, BS6, BS7, and using the K/Ar dating technique for BS10, VB1, VB3, and VB4. As all samples are basic in composition and lack K-rich minerals suitable for geochronology, the dating analyses were performed on groundmass. Fresh chips of the samples were crushed with a rigorously cleaned steel hydraulic press, sieved to a size fraction of 250–500 μm and rinsed in distilled $H_2O$ and in an ultrasonic bath to remove any dust or powder. In order to collect only the sample grains constituted by the groundmass, the sample fractions were handpicked under a binocular microscope to remove any phenocrysts (pyroxene and olivine). For $^{40}Ar/^{39}Ar$ analyses, after the irradiation in the TRIGA Reactor at the Oregon State University (USA), sample groundmass was analyzed at the Noble Gas Lab of the University of Vermont (USA) by laser step-heating using a Nu Instruments Noblesse magnetic sector noble gas mass spectrometer linked to an ultrahigh-vacuum extraction line powdered by a Santa Cruz Laser Microfurnace 75 W diode laser system. Age plateaus are defined by three or more consecutive steps within uncertainty encompassing 60% or more of the $^{39}Ar$, and all ages are reported with 2σ uncertainty. The K/Ar analyses were carried out at Actlabs in Canada. The determination of radiogenic Ar content was carried out twice on MI-1201 IG mass-spectrometer by isotope dilution method with $^{38}Ar$ as spike. Additional details about the geochronological analyses are reported in the Supplementary material.

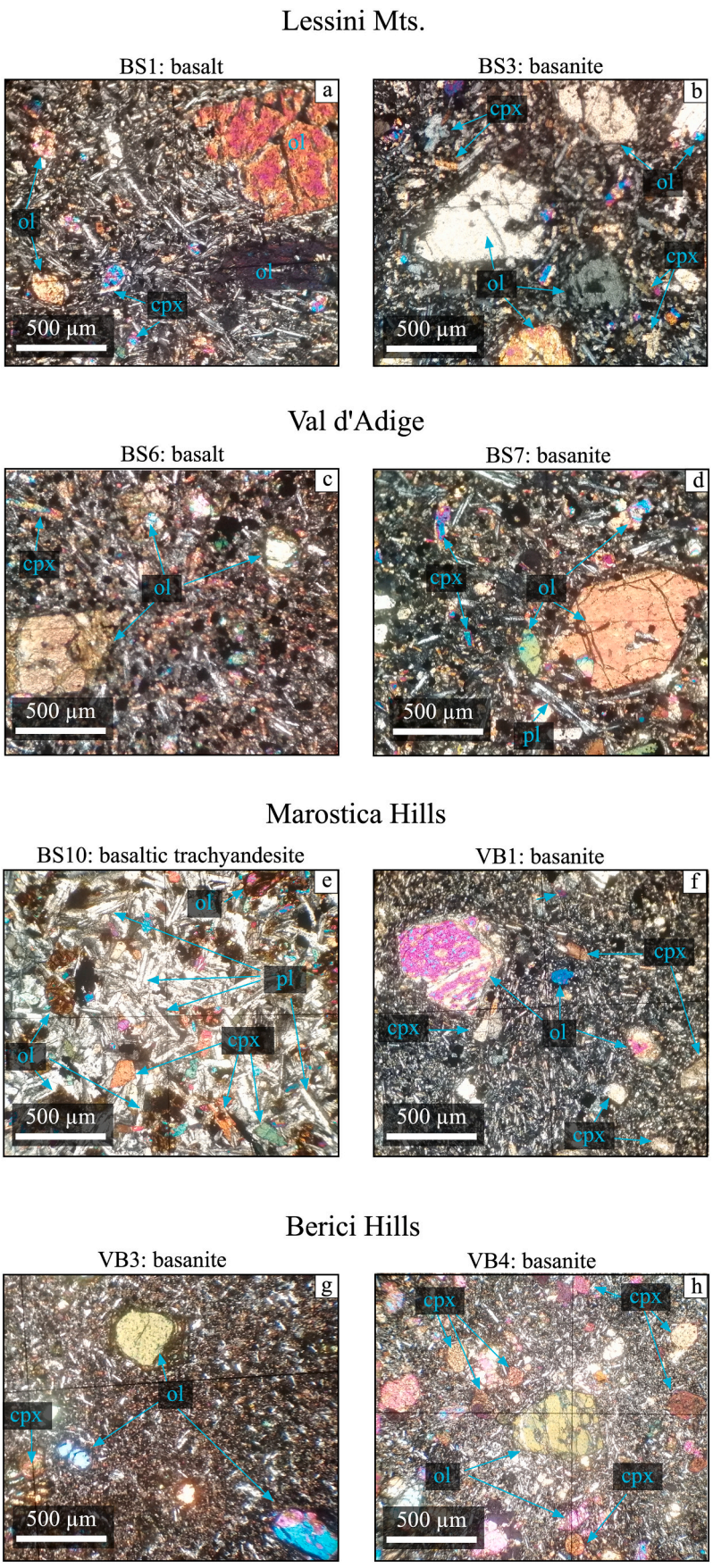


**Fig. 3.** Crossed-polarizers representative photomicrographs of the investigated VVP samples. Abbreviation: Ol = olivine, Cpx = clinopyroxene, Pl = plagioclase.

**Table 1**
Sr, Nd, Pb isotope composition of VVP samples.

| | Lessini Mts. | | | Val d'Adige | | Marostica Hills | Berici Hills | |
|---|---|---|---|---|---|---|---|---|
| Sample | BS1 | BS3 | BS10 | BS6 | BS7 | VB1 | VB3 | VB4 |
| Rock | Basalt | Basanite | Basaltic trachyandesite | Basalt | Tephrite | Basanite | Basanite | Basanite |
| $^{143}Nd/^{144}Nd$ | 0.512942 ± 5 | 0.512927 ± 5 | 0.512934 ± 6 | 0.512917 ± 7 | 0.512912 ± 4 | 0.512927 ± 4 | 0.512930 ± 4 | 0.512935 ± 4 |
| $^{87}Sr/^{86}Sr$ | 0.703250 ± 6 | 0.703192 ± 6 | 0.703303 ± 5 | 0.703295 ± 6 | 0.703234 ± 6 | 0.703283 ± 6 | 0.703222 ± 6 | 0.703212 ± 7 |
| $^{206}Pb/^{204}Pb$ | 19.4231 ± 3 | 19.5683 ± 4 | 19.4314 ± 3 | 19.4295 ± 2 | 19.4900 ± 3 | – | – | – |
| $^{207}Pb/^{204}Pb$ | 15.6555 ± 3 | 15.6588 ± 3 | 15.6562 ± 2 | 15.6658 ± 2 | 15.6623 ± 3 | – | – | – |
| $^{208}Pb/^{204}Pb$ | 39.2655 ± 7 | 39.3303 ± 9 | 39.2688 ± 6 | 39.2725 ± 5 | 39.3332 ± 7 | – | – | – |

## 4. Results

### 4.1. Rock classification, petrography, and mineral chemistry

According to the total alkali *vs.* silica (TAS) diagram (Le Maitre et al., 2002; Fig. 2a) the samples range between ultrabasic to basic compositions, with a general alkaline affinity. Samples BS3, BS6, BS7, VB1, VB3, and VB4 are classified as basanites on the TAS diagram, and they are nepheline-normative (Supplementary Table 2). They show porphyritic texture with euhedral/subhedral olivine (up to 2 mm across) and subordinate clinopyroxene (up to 0.5 mm across) as dominant phenocrysts set in a microcrystalline groundmass constituted by acicular plagioclase, clinopyroxene, and oxides (Fig. 3; Supplementary Table 2). Sample BS1 is classified as basalt according the TAS diagram and it is nepheline-normative (Supplementary Table 2). It is characterized by less and smaller olivine (up to 1 mm across) and clinopyroxene (up to 0.2 mm across) phenocrysts than those in basanites, within a groundmass including acicular plagioclase, clinopyroxene, oxides, and glass (Fig. 3a; Supplementary Table 2). Sample BS10 is classified as basaltic trachyandesite in the TAS diagram (Fig. 2a) and is hypersthene-normative (Supplementary Table 2). It is characterized by intergranular texture with elongated and euhedral plagioclase (up to 2 mm across) and subhedral clinopyroxene, olivine, and oxides filling spaces between plagioclase crystals (Fig. 3e; Supplementary Table 2).

The mineral compositions of olivine, clinopyroxene, and plagioclase are quite homogeneous among the sample population. The Fo [$100 \times Mg/(Mg + Fe)_{mol}$, where Fe is total iron] content of olivine phenocrysts of samples BS3, BS6, BS7, VB3, and VB4 range from 71.8 to 83.1; only VB1 has higher Fo contents ranging from 82.6 to 88.7. The clinopyroxene crystals are all diopside, with $Wo_{47–53}$ $En_{32–41}$ $Fs_{10–15}$ and Mg# [$100 \times Mg/(Mg + Fe)_{mol}$, where Fe is total iron] varying from 69.4 to 80.2, with no significant variation from core to rim. Only clinopyroxenes of VB1 have a composition slightly different ($Wo_{45–47}$ $En_{42–43}$ $Fs_{8–9}$) and higher Mg# (~82). For all samples, the microphenocrysts of plagioclase have an andesine composition ($An_{49}$ to $An_{64}$). Noteworthy, samples BS1, BS3, VB1 and VB4 host small (2–3 cm) mantle peridotite xenoliths, similar to those described in other VVP sample suites (Beccaluva et al., 2001; Brombin et al., 2018; Gasperini et al., 2006; Morten et al., 1989; Siena and Coltorti, 1989, 1993).

### 4.2. Geochemistry

Whole rock major and trace element compositions are reported in Supplementary Table 2. On the TAS diagram the investigated samples have $SiO_2$-alkali contents similar to the other VVP rocks having a relatively primitive character (Beccaluva et al., 2007; Brombin et al., 2019; Macera et al., 2003; Milani et al., 1999; Fig. 2a). In fact, samples of this study have low $SiO_2$ (42.6 to 51.2 wt%), high MgO (12.4 to 7.7 wt%) contents, and high Mg# (67.8 to 57.2, Supplementary Table 2). The samples have alkaline compositions, except for BS10, which straddles alkaline and subalkaline fields in the TAS diagram. The samples BS3, BS7, BS10, VB1, VB3, and VB4 have sodic character [$(Na_2O - K_2O) \geq 2.0$ wt%] with ($Na_2O - K_2O$) ranging from 2.03 wt% to 3.89 wt%, while samples BS1 and BS6 show a slight potassic affinity, as ($Na_2O - K_2O$) values are 1.82 wt% and 1.49 wt%, respectively. Compatible trace elements have relatively high concentration with Ni varying from 102 to 310 ppm, Co from 42 to 76 ppm, Cr from 170 to 432 ppm, V from 159 to 298 ppm, which confirm that samples are relatively undifferentiated (Supplementary Table 2).

In terms of incompatible trace elements, the samples of this study overlap with the VVP rocks investigated in literature (Beccaluva et al., 2007; Brombin et al., 2019; Macera et al., 2003; Milani et al., 1999). The primordial mantle-normalized (McDonough and Sun, 1995) incompatible trace element patterns of basanites (BS3, BS6, BS7, VB1, VB3, VB4) and basalt (BS1), are nearly parallel (Fig. 2b). These samples display Light (L-) Rare Earth Element (REE) enrichment and a LREE to Heavy (H-) REE fractionation [$(La/Yb)_N$: 14.22–23.37; $(Dy/Lu)_N$: 2.19–2.86; Fig. 2b]. They also exhibit negative K, Rb, Zr, Hf, and Ti anomalies as well as positive Ba and P anomalies.

The basaltic trachyandesite (BS10), *i.e.*, the least alkaline rock of this sample suite, mimics - at lower concentration - the general trace element pattern of other VVP rocks, showing a steeper negative slope from Nb to Y and the lack of positive Ba and negative Rb anomalies (Fig. 2b).

The Sr-Nd-Pb isotopic ratios are listed in Table 1.

The VVP magmatic products of this study are characterized by low $^{87}Sr/^{86}Sr$ (0.70319–0.70330; Fig. 4a, b) and high $^{143}Nd/^{144}Nd$ (0.512912–0.512942; Fig. 4a, b), which fall into the isotopic ranges of the majority of VVP basic-ultrabasic magmatic products studied in literature ($^{87}Sr/^{86}Sr$: 0.70315–0.70386; $^{143}Nd/^{144}Nd$: 0.51285–0.51298; Beccaluva et al., 2007; Macera et al., 2003; Fig. 4a, b).

The Pb isotopes exhibit a narrow variability ($^{206}Pb/^{204}Pb$: 19.423–19.568; $^{207}Pb/^{204}Pb$: 15.656–15.666; $^{208}Pb/^{204}Pb$: 39.266–39.333; Fig. 4c–f), included in the compositional range described by previous authors ($^{206}Pb/^{204}Pb$: 18.786–19.760; $^{207}Pb/^{204}Pb$: 15.580–15.670; $^{208}Pb/^{204}Pb$: 38.807–39.490; Beccaluva et al., 2007; Macera et al., 2003; Fig. 4c–f). In Pb—Pb spaces (Fig. 4c–f), the VVP samples of this study define a linear trend above the Northern Hemisphere Reference Line (NHRL; Hart, 1984). In particular, in the $^{206}Pb/^{204}Pb$ *vs* $^{207}Pb/^{204}Pb$ plot (Fig. 4c, d) the basanites (BS3, BS6, BS7) define a perpendicular trend above the NHRL with the BS3 and BS6, as the nearest and the furthest samples from the NHRL, respectively. The basalt (BS1) and the basaltic trachyandesite (BS10) are off this trend, having lower $^{207}Pb/^{204}Pb$ values (15.655–15.656; Table 1) with respect to the remaining samples of the suite (15.658–15.665; Table 1). In the $^{206}Pb/^{204}Pb$ *vs* $^{208}Pb/^{204}Pb$ plot (Fig. 4e, f), BS1, BS6, BS7, and BS10 define a parallel trend above the NHRL, only sample BS3 is off this trend, plotting just off the NHRL.

### 4.3. $^{40}Ar/^{39}Ar$ and K/Ar geochronological constraints

In order to place age constraints on the emplacement in the oldest VVP districts (*i.e.*, Lessini Mts. and Val d'Adige), samples BS1, BS3, BS6, and BS7 were evaluated for $^{40}Ar/^{39}Ar$ age. The results of the analyzed VVP samples and the estimated ages are reported in Table 2.

Almost all inverse isochrons yielded $^{40}Ar/^{36}Ar$ intercepts similar to

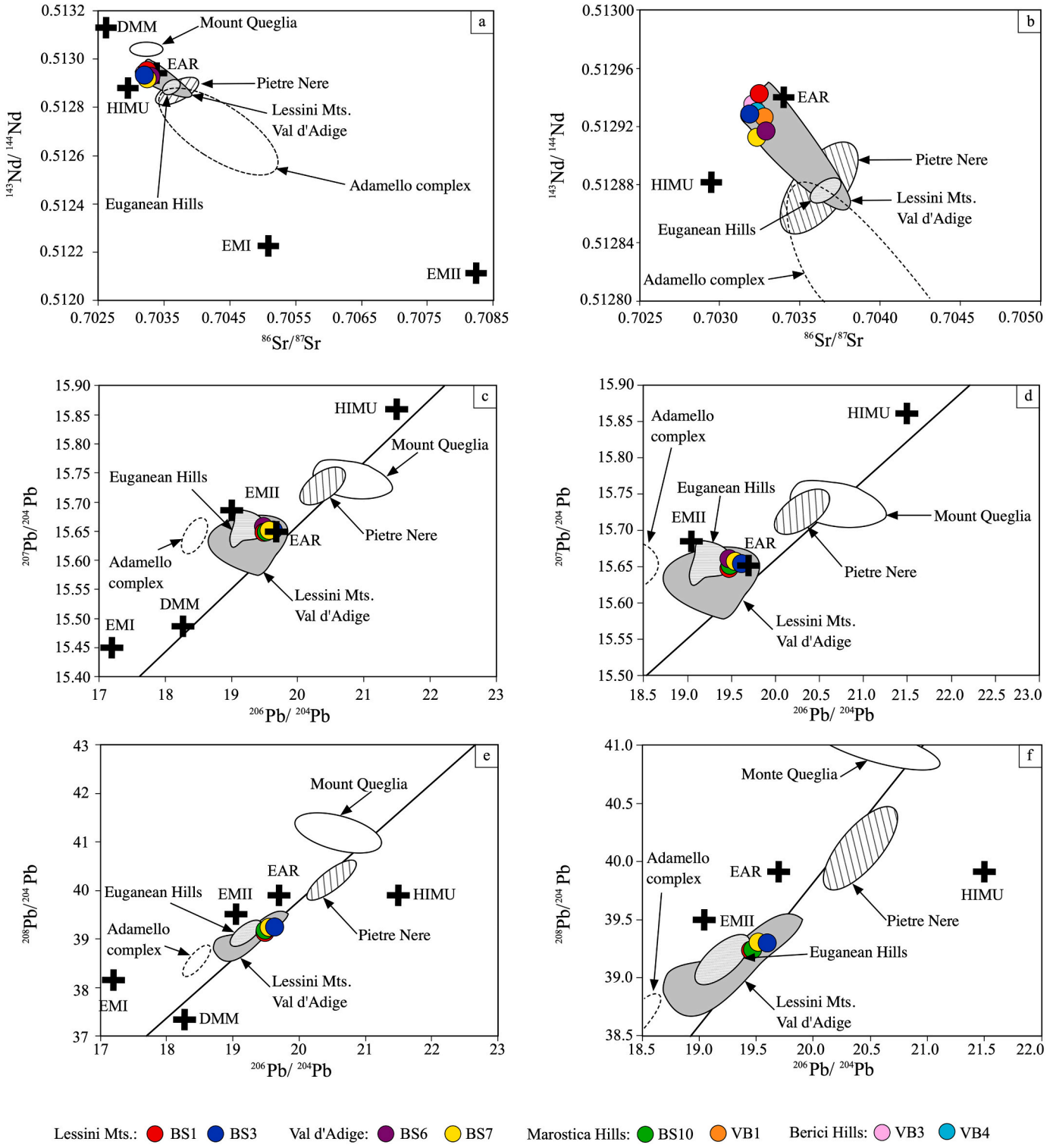


**Fig. 4.** Sr-Nd-Pb isotopic composition of VVP samples studied in this work (large symbols) compared with those of VVP products retrieved from the literature (Beccaluva et al., 2007; Macera et al., 2003; Milani et al., 1999), those of other Cenozoic volcanic occurrences (Mount Queglia, Pietre Nere) of the Adria microplate (Bianchini et al., 2008), and those of basic dykes from the Adamello plutonic complex (Hürlimann et al., 2016). Fig. b, d, and f are zoom portions of a, c, and e, respectively.

Geochemical components depleted mantle (DMM), HIMU (high U/Pb = high μ), EMI and EMII (enriched mantle) are after Zindler and Hart (1986); European Asthenospheric Reservoir (EAR) is after Cebriá and Wilson (1995). The Northern Hemisphere Reference Line (NHRL) is from Hart (1984).

the atmospheric value (298.56 ± 0.31; Lee et al., 2006), indicating that the analyzed rocks did not have trapped excess argon. For the Lessini Mts. samples, the basalt BS1 has a $^{40}Ar/^{36}Ar$ intercepts indistinguishable from the atmospheric ratio (299 ± 64; Fig. 5a) and yielded a mini-plateau age of 42.76 ± 1.70 Ma [mean square weighted deviation (MSWD) = 1.9; probability (p) = 0.10; Fig. 5b), as it based on 60% of the total gas. For the basanite BS3, the geochronological analysis was repeated twice, as the first analysis did not result in a plateau age;

**Table 2**
Summary of $^{40}Ar/^{39}Ar$ results for VVP samples.

| | | Isochron characteristics | | | Plateau characteristics | | | | |
|---|---|---|---|---|---|---|---|---|---|
| | | Inverse isochron age (Ma, ±2σ) | $^{40}Ar/^{36}Ar$ intercept (±2σ) | MSWD | Plateau age (Ma, ±2σ) | Total $^{39}Ar$ released (%) | p | MSWD | n (N) |
| Lessini Mts. | | | | | | | | | |
| BS1 | Basalt | 44.4 ± 10.4 | 299 ± 64 | 4.9 | 42.76 ± 1.70 | 60 | 0.10 | 1.9 | 5 (10) |
| BS3 (first test) | Basanite | *45.9* | *125* | *2.4* | *No plateau age* | | | | |
| BS3 (second test) | Basanite | *43* | *164* | *65.0* | *No plateau age* | | | | |
| Val d'Adige | | | | | | | | | |
| BS6 | Basanite | 41.9 ± 2.0 | 282 ± 38 | 0.7 | 41.73 ± 0.84 | 97 | 0.07 | 2.2 | 5 (6) |
| BS7 | Basanite | 42.8 ± 3.0 | 182 ± 100 | 7.4 | 41.21 ± 1.76 | 92 | 0.00 | 5.3 | 8 (9) |

Mean square weighted deviations (MSWD) for inverse isochrons and plateau ages, $^{40}Ar/^{36}Ar$ intercepts, percentage (%) of $^{39}Ar$ degassed used in the plateu calculation, probability (p) for plateau ages, and number of heating steps included in the plateu age. Analytical uncertainties on the ages and $^{40}Ar/^{36}Ar$ intercepts are quoted at 2 sigma (2σ) confidence levels. Data in italics indicate results that have to be taken with caution because of disturbed spectra.

however, in the first test the maximum apparent age of the steps was ~45 Ma (Fig. 5d) as confirmed by the inverse isochron age (Fig. 5c). In the second test the maximum apparent age of the steps was ~43 Ma (Fig. 5f), again confirmed by the respective inverse isochron age (Fig. 5e), indicating that the apparent age of this sample is between 43 and 45 Ma. For this sample we are more prone to consider the oldest age (~45 Ma) more valid, rather than the youngest age (~43 Ma), as the corresponding inverse isochron has the lowest error (Fig. 5c); additionally, another basanite collected in the same locality was analyzed by Brombin et al. (2019) and yielded both plateau age and inverse isochron age of 45 Ma. For the Val d'Adige samples: the basanite BS6 is characterized by a $^{40}Ar/^{36}Ar$ intercept indistinguishable from the atmospheric ratio (282 ± 38; Fig. 5g), which results in a calculated plateau age of 41.73 ± 0.84 Ma (MSWD = 2.2; $p = 0.07$; Fig. 5h) accounting for 90% released $^{39}Ar$. For the basanite BS7 the $^{40}Ar/^{36}Ar$ intercept was sub-atmospheric (182 ± 100; Fig. 5i), indicating argon loss probably due to the alteration. Its apparent age spectra yielded a plateau age of 41.21 ± 1.76 Ma (MSWD = 5.3; Fig. 5j) including 90% of the released $^{39}Ar$.

The data set was integrated with additional K/Ar geochronological data on samples BS10, VB1, VB3, and VB4 (Table 3), constraining the timeframe of magmatic activities occurred in Berici Hills and Marostica Hills districts, which although are poorly investigated by previous studies, was considered younger with respect to those of the Lessini area.

For the Marostica Hills, the basaltic trachyandesite BS10 collected in the western edge of the district recorded an age of 32.5 ± 1.2 Ma, and the basanite VB1 from the neck of Monte Gloso yielded an age of 26.7 ± 0.8 Ma. The latter age tends to that reported in literature by Brombin et al. (2019), which dated other two samples from the same location and obtained $^{40}Ar/^{39}Ar$ ages of ~22 Ma. For the Berici Hills the two basanites VB3 and VB4 yielded indistinguishable ages of 39.9 ± 1.5 and 39.2 ± 1.5 Ma, respectively.

## 5. Discussion

### 5.1. Mantle source characteristics

Despite the fact that the VVP magmatism was distributed in five magmatic districts over an area of ~1500 $km^2$ in the Southeastern Alpine domain, the magmatic products show a consistent intraplate character, as well as very homogeneous trace element and isotopic features (Figs. 2b, 4). In addition, the mineral compositions of olivines, clinopyroxenes, and plagioclases are also homogenous across our sample suite, emphasizing that the VVP districts share similar parental melts, and plausibly mantle source(s) and melting conditions. The VVP samples frequently entrain mantle xenoliths, thus indicating a rapid ascent from the mantle source region, without stagnation in crustal magma chambers. This hypothesis is corroborated by the small difference (a few tens of °C) between the temperature at which VVP melts were segregated from the mantle, which is 1370 °C on average, based on the algorithm defined by Albarede (1992), and the olivine liquidus temperature extrapolated by the Roeder and Emslie (1970) geothermometer. Coherently, the trace element patterns and positive and negative anomalies of the VVP samples should be interpreted as features inherited by mantle sources, considering the primitive character of the rocks. In Fig. 2b, the patterns are similar to the Ocean Island Basalt (OIB; Sun and McDonough, 1989) trend and consistent with the intraplate features already noticed in previous studies (Beccaluva et al., 2007; Brombin et al., 2019; Macera et al., 2003; Milani et al., 1999). Based on trace elements, Beccaluva et al. (2007) invoked as potential source a spinel lherzolite enriched by hydrated-carbonated components. On the contrary, Brombin et al. (2019) proposed a garnet lherzolite possibly metasomatized by carbonatitic melts and with residual phlogopite as a potential source, which is more consistent with the trace element patterns observed from the samples of this study. In fact, VVP products exhibit the steep Middle (M-) HREE profiles typical of a garnet signature, as well as K, Rb depletions indicating a K (Rb)-bearing residual phase, like phlogopite or amphibole, in the mantle source (*e.g.*, Moine et al., 2001) (Fig. 2b). According to LaTourette et al. (1995), melts formed from amphibole-bearing peridotites have higher Ba/Rb (> 50) than melts of a phlogopite-bearing peridotites (Ba/Rb < 20). Most VVP samples exhibit low Ba/Rb values (10 to 20), which indicate the presence of residual phlogopite within their mantle source. Only Berici Hills basanites (VB3 and VB4) show very high Ba/Rb (> 100), which suggest a mantle source with amphibole rather than phlogopite as residual phase. However, despite the possible mineralogical differences in the relative mantle sources, all VVP samples are invariably characterized by Ba and P enrichments, which recall metasomatism by carbonatitic fluids (Merle et al., 2017).

In order to investigate further the possible nature of the VVP mantle source, the Sr, Nd, and Pb isotopes presented in this study were compared with those previously reported in the literature (Beccaluva et al., 2007; Macera et al., 2003). The analyzed VVP samples are characterized by low $^{87}Sr/^{86}Sr$ and high $^{143}Nd/^{144}Nd$ isotopic ratios that are consistent with the previous investigations (Beccaluva et al., 2007; Macera et al., 2003; Milani et al., 1999; Fig. 4a, b). Only few samples from Lessini Mts. and Euganean Hills from the literature record higher $^{87}Sr/^{86}Sr$ (up to 0.70386) and lower $^{143}Nd/^{144}Nd$ (up to 0.51285) isotopic compositions, due to sporadic shallow level crustal contamination during magma upraising and emplacement (Macera et al., 2003). In the Sr—Nd diagram, all samples of our suite are close to the HIMU mantle, and cluster near the EAR (European Asthenospheric Reservoir; Cebriá and Wilson, 1995; Hoernle et al., 1995; Wilson and Downes, 2006). The Pb isotopic values confirm this fingerprint, as the VVP samples plotted between DMM and HIMU components, and also in this case are near the

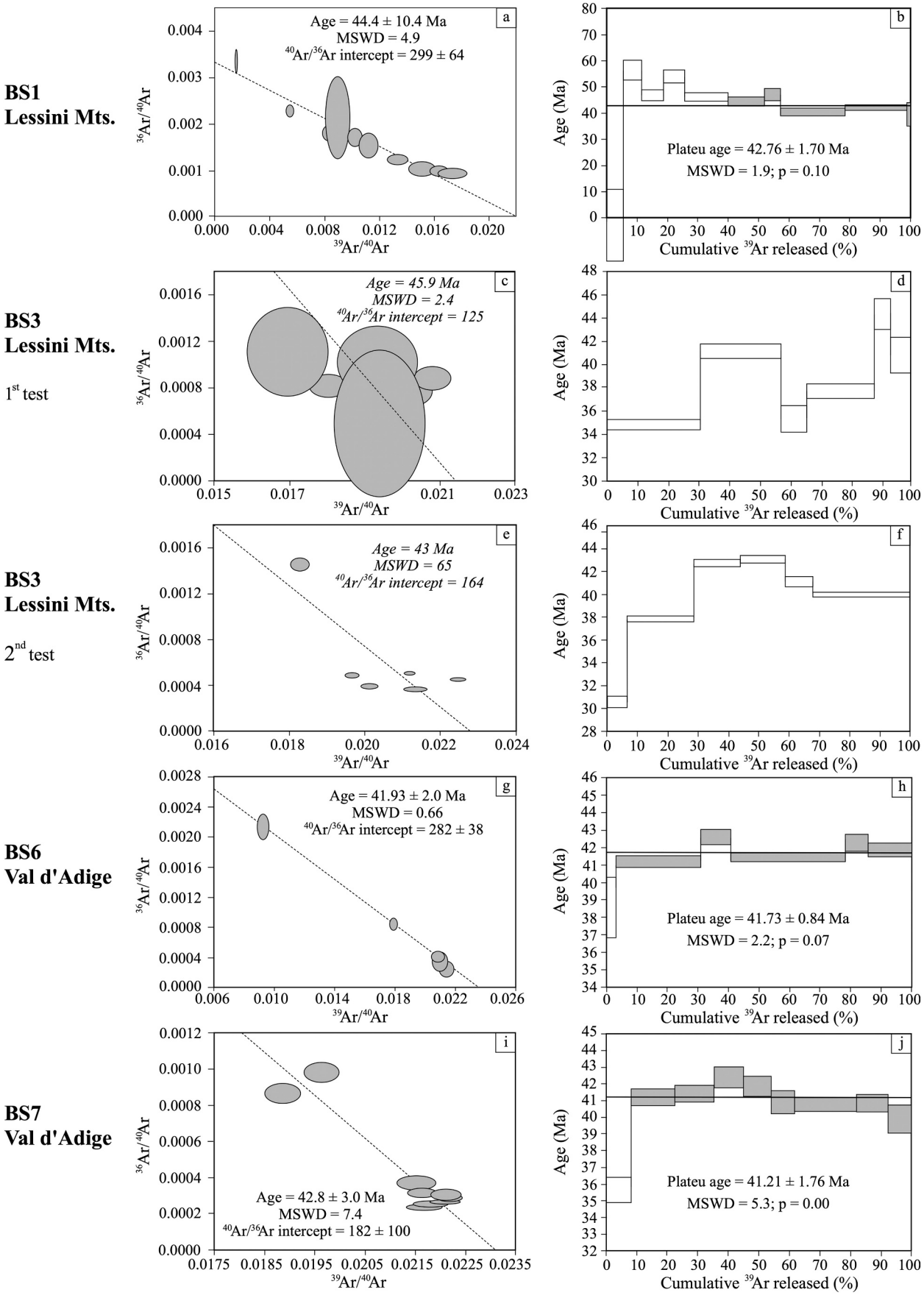


**Fig. 5.** $^{39}Ar/^{40}Ar$ *vs* $^{36}Ar/^{40}Ar$ inverse isochrons and $^{40}Ar/^{39}Ar$ apparent age spectra plotted against the cumulative percentage of $^{39}Ar$ released for VVP samples. For the geochronological analysis which did not result in a plateau age, ages are reported in italics.

**Table 3**
Summary of K/Ar results for VVP samples.

| | | K (% ± 2σ) | $^{40}$Ar radiogenic (ng/g) | Age (Ma, ± 2σ) |
|---|---|---|---|---|
| Marostica Hills | | | | |
| BS10 | Basaltic trachyandesite | 1.17 ± 0.02 | 2.66 ± 0.03 | 32.5 ± 1.2 |
| VB1 | Basanite | 0.694 ± 0.010 | 1.294 ± 0.009 | 26.7 ± 0.8 |
| Berici Hills | | | | |
| VB3 | Basanite | 0.524 ± 0.010 | 1.468 ± 0.009 | 39.9 ± 1.5 |
| VB4 | Basanite | 0.564 ± 0.010 | 1.552 ± 0.014 | 39.2 ± 1.5 |

Potassium concentration in percent, radiogenic argon in ng/g. Ages (Ma) analytical uncertainties are quoted at 2 sigma (2σ) confidence levels.

EAR. The EAR is a regional sub-lithospheric mantle component extending from the eastern Atlantic to Europe and the Mediterranean area (Bianchini et al., 1999; Wilson and Bianchini, 1999), which is also known in literature as the low-velocity component (LVC; Hoernle et al., 1995), or Common Mantle Reservoir (CMR; Lustrino and Wilson, 2007). The EAR was invoked for other intraplate Late Cretaceous-Cenozoic magmatic occurrences from the Adria microplate, such as the Pietre Nere and Mount Queglia dikes (Bianchini et al., 2008). The Sr-Nd-Pb isotopic fingerprint of VVP rocks, approaching those of other intraplate magmatic districts of the Mediterranean area, indicates that the VVP mantle sources were unaffected by the Cenozoic subduction-related processes which occurred in the Alpine domain (Bianchini et al., 2008; Wilson and Bianchini, 1999). There are several cases worldwide documenting the presence of intraplate-like magmatism near subduction zones (especially in the circum-Mediterranean area; Beccaluva et al., 2011), and the geodynamic interpretations are various and still matter of debate in the geological literature. In the following section we present a new geodynamic model inferred by the timing of the VVP intraplate magmatic activities and the coeval magmatic orogenic activities along the Periadriatic line.

### 5.2. *Temporal and volume distribution of VVP magmatic activities: Constraints for a new geodynamic model*

According to the temporal reconstruction of the VVP provided by the past studies, the magmatism occurred intermittently for a very long period (~40 My), starting from the Paleocene in the Lessini Mts. and Val d'Adige districts (Barbieri, 1972; Medizza, 1965) and then migrating East (Bassi et al., 2008; Brombin et al., 2019; De Vecchi and Sedea, 1995). During the middle Eocene magmatic activity still occurred in the Lessini Mts. and Val d'Adige districts and started in the Berici Hills district. In the late Eocene, basic magmatism occurred in the Euganean Hills, while during the Oligocene differentiation processes become preponderant and produced acidic products. At this time, the magmatism started also in the Marostica Hills, where it likely continued until the Miocene (Bassi et al., 2008; Brombin et al., 2019; De Vecchi and Sedea, 1995). In this study, for the first time, radioisotopic ages of samples collected in the Berici Hills testify the occurrence of magmatic activities during middle Eocene in this district. In addition, the K/Ar ages of samples collected in the Marostica Hills: i) verify the occurrence of magmatism in the Oligocene at least in the western border of this district and ii) confirm also the presence of magmatic events in the Miocene, as tentatively proposed by Brombin et al. (2019). The $^{40}$Ar/$^{39}$Ar radioisotopic ages carried out in this work unequivocally confirm that the eruptions in Lessini Mts. and Val d'Adige appeared at ~45 Ma and ~ 42 Ma, respectively. Therefore, combining the recent $^{40}$Ar/$^{39}$Ar dating from Brombin et al. (2019) with those from this study, the oldest magmatism occurred in the Lessini Mts. can be dated to ~45 Ma, at the latest. This suggests that the onset of the VVP magmatism was in the middle Eocene, and not in the Paleocene. Thus, the time-span of the VVP magmatism was much shorter than what previously hypothesized in the literature only on the basis of stratigraphic evidence recorded in the 1960s and 1970s (Barbieri, 1972; Medizza, 1965) without an independent confirmation by new biostratigraphic and/or radioisotopic geochronological constraints.

According to the literature, the Eocene magmatism in Lessini Mts. and Val d'Adige districts corresponds with the most intense VVP magmatic pulse, as the highest volumes of the VVP products erupted in this zone. In order to test this interpretation, which is fundamental for the geodynamic reconstruction of the mechanism responsible of the VVP magmatism, we estimated the volume of magmas of each VVP district. For the calculation we used an approach similar to that of Svensen et al. (2018), which estimated the sill volumes of Central Atlantic Magmatic Province. For this calculation we measured the aerial extent of the present-day magmatic outcrops of each VVP district and the average thickness of volcanic formation reported in field observations and stratigraphic columns (Brombin et al., 2019). We determined the volumes of magmatic products hosted in Lessini Mts., Euganean Hills, and Marostica Hills districts (Fig. 6a; Supplementary Table 3), while we did not perform the calculation for Val d'Adige and Berici Hills districts, where the aerial extents are totally subordinate. According to Fig. 6a, the amount of the magmatic products decreases in the VVP following the order Lessini Mts. > Euganean Hills > Marostica Hills, which suggests that the volume of magmas decreases toward East and also for the youngest VVP districts. Therefore, the paroxysm of the VVP magmatism occurred in the Eocene in the Lessini Mts., as the estimated volume of magmatic products is 36 km$^3$ (Fig. 6a; Supplementary Table 3) and then it waned toward the East during Oligocene and Miocene, when eruptions occurred in Euganean Hills and Marostica Hills districts, where we estimated 25 and 8.4 km$^3$ of magmatic products, respectively (Fig. 6a; Supplementary Table 3).

Interestingly, the climax of VVP activity in the Eocene was nearly contemporaneous with the emplacements of magmatic orogenic intrusive bodies along the Periadriatic lineament, in particular those close to the Giudicarie fault system, as shown by the Adamello intrusive complex emplaced at ~43 Ma (Ji et al., 2019; Schaltegger et al., 2019; Fig. 6a), when Alpine subduction and continental collision was still ongoing, as demonstrated by the existence of eclogitic units formed in the same period (peak metamorphic age: ~45–40 Ma Lapen et al., 2007; Malusà et al., 2011; Rubatto et al., 1998; Rubatto and Hermann, 2001; Wiederkehr et al., 2009).

Several authors have tried to explain the peculiar geodynamic framework which led to the occurrence of intraplate magmas in the VVP in proximity of a subduction zone during the general Alpine convergence. Among the distinct theories, the VVP was interpreted as a "passive impactogenic rift" (Barberi et al., 1982; Mats and Perepelova, 2011), where activation of transtensional lineaments and decompressional melting occurred as foreland reactions to the general Alpine convergence (Beccaluva et al., 2007, 2011). Other interpretations favoured magma genesis induced by mantle uprising through a slab window after the European slab breakoff (Macera et al., 2003). In their recent study, Brombin et al. (2019) discarded the slab breakoff as the triggering mechanism of magma genesis considering recent tomographic images and geophysical data, which evidenced a continuous nearly vertical slab, beneath the northern edge of the South Alpine region (Hua et al., 2017; Kästle et al., 2020; Zhao et al., 2016). According to plate-tectonic reconstructions of Handy et al. (2010, 2015) based on stratigraphic, petrological, geochronological data and seismic tomography, the slab beneath the Alpine region was nearly vertical since 67 Ma, *i.e.*, before the onset of the VVP magmatism. The presence of a poloidal mantle flow bypassing the Alpine slab deepening southward was thus suggested, providing the upraise of deep mantle domains unaffected by subduction-related fluids beneath the South Alpine region (Brombin et al., 2019). The last model does not imply a horizontal slab breakoff as proposed by Davies and von Blanckenburg (1995) and Macera et al. (2003) but requires a "vertical" segmentation of the European slab in distinct sectors that are divided by important translithospheric discontinuities that offset the Alpine belt. The hypothesis is

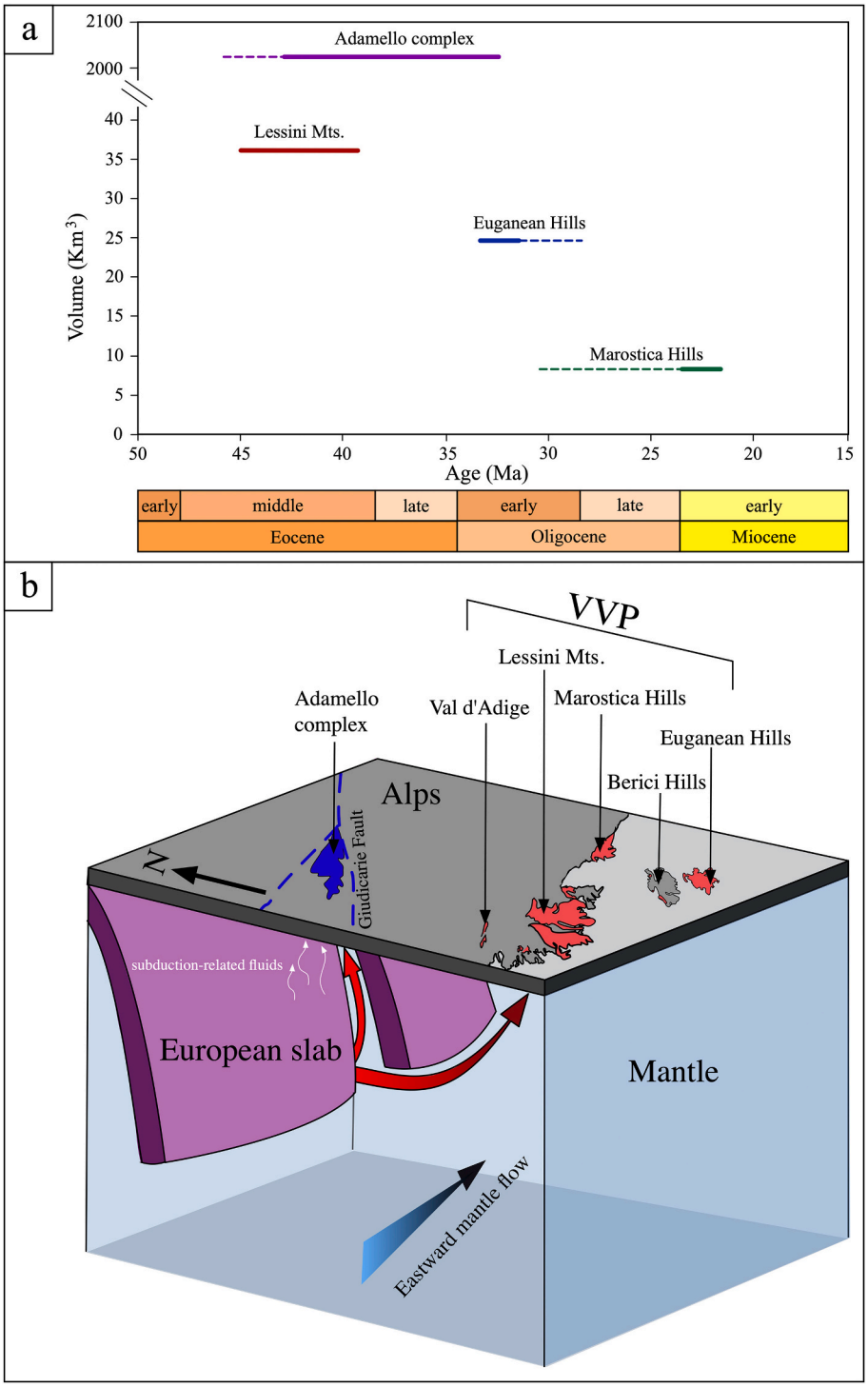


**Fig. 6.** a) Average volumes of magmatic products occurred in Lessini Mts., Euganean Hills, and Marostica Hills districts from Eocene to Miocene (this work) and average volume of magmatic products occurred in the Adamello complex from Eocene to Oligocene (Schaltegger et al., 2019). The dotted lines indicate the ages of magmatic activities, that should be considered questionable, as derived from old K—Ar or Rb—Sr dating techniques, which are less reliable than Ar—Ar method (see Brombin et al., 2019 for a review). b) Schematic cartoon (not in scale) for the magmatism of Adamello complex along the Periadriatic Line (Central Alps) and the VVP (Southeastern Alps) during Eocene-Oligocene. Through the vertical slab tear, located near the Giudicarie fault zone, upwelling mantle with a poloidal flow melted and led to Adamello complex magmatism. Coherently with the general Earth mantle flow, the poloidal flow migrated toward East and also triggered the intraplate magmatism in the VVP.

compatible with the most recent interpretations of the Alpine architecture based on geophysical data (Hua et al., 2017; Kästle et al., 2020; Zhao et al., 2016), which emphasized a sharp translithospheric discontinuity (possibly a vertical slab tear) at the boundary between Central and Eastern Alps. In our view (Fig. 6b), to reconcile the location of most orogenic magmatism along the Periadriatic lineament, which is concentrated in the Adamello complex, and the VVP intraplate magmatism, the vertical slab tear should be located in correspondence of the Giudicarie fault zone, and according to the magmatic timing, its rupture plausibly occurred in the middle Eocene. This agrees with what suggested by Castellarin et al. (2006) that emphasized a deep continuation of the Giudicarie lineament and its long-lived activity.

In the lithospheric region, the vertical split between the two slab segments allowed the upwelling of a deep poloidal asthenospheric mantle flow, whereas the deep lithospheric region near the slab was likely affected by subduction-related fluids (Fig. 6b). Then, the poloidal mantle flow triggered the partial melting in the mantle source(s) near the subduction slab, producing the orogenic (fluid-dominated?) signature that characterized the Adamello magmatic products (Fig. 6b). The asthenospheric poloidal mantle flow migrated toward East following the general eastward mantle flow (Ficini et al., 2017; Petrescu et al., 2020) and triggered the decompressional melting of the VVP mantle source,

which remained unaffected by the subduction-related fluids due to its position far from the slab (Fig. 6b) and developed the observed intraplate signature. Therefore, the Giudicarie fault system represents the surface expression of an important lithospheric discontinuity activated in the middle Eocene. This discontinuity could be responsible for triggering orogenic magmatism in the Eocene along the Periadriatic Line, at least in the Central Alps domain (*e.g.*, Adamello complex), and the synchronous intraplate magmatism in the western VVP districts (Lessini Mts. and Val d'Adige).

After the main magmatic pulse during middle Eocene in the Lessini sector, the volcanism migrated eastward and southeastward in the Euganean and Marostica Hills, where magma genesis resumed in the Oligocene and Miocene times, respectively. This spatio-temporal evolution of the volcanism is possibly related to the mantle poloidal flow, which transferred fertile mantle domains at velocity between 0.5 and 1 cm $y^{-1}$, estimated considering the distance between Lessini Mts. and Euganean/Marostica Hills districts and the time elapsed between the respective eruptions. This velocity estimate of the lateral mantle flow in subduction systems is of the same order of what was proposed by Funiciello et al. (2004) on the basis of 3D laboratory experiments. Noteworthy, the importance of slab tears in controlling a) convective mantle cells around slabs and b) triggering of magmatic occurrences variously influenced (or even not influenced) by subduction related fluids has been convincingly proposed by Faccenna et al. (2007). Such process seems to be effective to explain the Cenozoic spatio-temporal association of volcanic products having distinct magmatic affinity in and around the Italian peninsula (*e.g.*, Southern Tyrrhenian, Sicily; Gvirtzman and Nur, 1999; Bianchini et al., 2008; De Ritis et al., 2019; Barreca et al., 2020), as well as to explain the occurrence of post-collisional intraplate magmatism in other areas of the world, *e.g.*, in the Western Anatolia (Dilek and Altunkaynak, 2009; Prelević et al., 2015) and East Carpathian (Bracco Gartner et al., 2020).

## 6. Conclusions

The Veneto Volcanic Province (VVP) magmatic products in the Southeastern Alpine domain exhibit a geochemical and isotopic intraplate signature despite its proximity to subduction-related magmatism that occurred along the Alpine belt as a consequence of the Europe-Adria convergence. The trace element patterns of the investigated VVP magmatic products point to a garnet-peridotite mantle source affected by carbonatitic fluids that stabilized metasomatic phases such as phlogopite or amphibole. The Sr-Nd-Pb isotopic signatures of the VVP lavas have similar features to those of other Cenozoic intraplate magmatic provinces of the Adria microplate, whose mantle sources were ascribed to the European Asthenospheric Reservoir, with no apparent contributions of subduction-related fluids.

Because of the complexity of the geophysical data and tomographic images of the Alpine architecture, the mechanism responsible for the occurrence of the intraplate magmatism of the VVP is still a matter of debate. One of the crucial issues is related to the onset of VVP magmatism. New $^{40}Ar/^{39}Ar$ geochronological dating presented in this study indicate the oldest magmatic activity occurred in the Eocene (~45 Ma) rather than in Paleocene, as has been hypothesized in previous studies. Therefore, the onset of VVP magmatism coincided with the Europe-Adria continental collision, which triggered the Alpine orogenesis and the orogenic magmatism along the Periadriatic lineament, in particular close to the Giudicarie Fault, where the Adamello intrusive complex emplaced. Considering these findings, a new geodynamic model is proposed: the Giudicarie Fault is the superficial expression of a vertical lithospheric discontinuity activated in the middle Eocene. This slab tear was responsible for the uprising of an asthenospheric poloidal mantle flow, which migrated toward East at velocities between 0.5 and 1 cm $y^{-1}$, following the general flow of the Earth's mantle. Then the poloidal flow triggered the decompressional melting of the mantle source beneath the VVP region inducing first the main magmatic pulse in the Lessini Mts. district at ~45 Ma, and other pulses also in Val d'Adige and Berici Hills during middle Eocene, whereas minor pulses in the Euganean and Marostica Hills occurred only during Oligocene and Miocene.

## Funding

Funding for this research was provided by University of Ferrara (FAR fund of GB), NSF-1255888 to JGB and IROP funding to EAP, United States National Science Foundation grant EAR 1028991 to LEW.

## Declaration of Competing Interest

The authors declare that they have no known competing financial interests or personal relationships that could have appeared to influence the work reported in this paper.

## Acknowledgements

We thank Renzo Tassinari (University of Ferrara) and Maurizio Mazzucchelli (University of Modena and Reggio Emilia) for geochemical analyses, Marcello Serracino (CNR-IGAG, Rome) for EMPA analyses, and Mahdi Ghobadi (Actlabs) for K/Ar analyses. We also thank the two reviewers, Dr. Matt Brueseke and Dr. Iain Neill, for their constructive criticism which improved the earlier version of the manuscript, as well as Dr. Greg Shellnutt for the thoughtful editorial handling.

## Appendix A. Supplementary data

Supplementary data to this article can be found online at https://doi.org/10.1016/j.lithos.2021.106507.

## References

Albarede, F., 1992. How deep do common basaltic magmas form and differentiate? J. Geophys. Res. 97, 10997–11009.
Avanzinelli, R., Boari, E., Conticelli, S., Francalanci, L., Guarnieri, L., Perini, G., Petrone, C.M., Tommasini, S., Ulivi, M., 2005. High precision Sr, Nd, and Pb isotopic analyses using new generation thermal ionisation mass spectrometer: aims and perspective for isotope geology applications. Period. Mineral. 74, 147–166.
Barberi, F., Santacroce, R., Varet, J., 1982. Chemical aspects of rift magmatism. In: Palmason, G. (Ed.), Continental and Oceanic Rifts. American Geophysical Union, Washington, DC, pp. 223–258.
Barbieri, G., 1972. Sul significato geologico della faglia di Castelvero (Lessini veronesi). In: Atti e Memorie Accademiche Patavina SS.LL.AA, 84, pp. 297–302.
Barreca, G., Branca, S., Corsaro, R.A., Scarfì, L., Cannavò, F., Aloisi, M., Monaco, C., Faccenna, C., 2020. Slab detachment, mantle flow, and crustal collision in eastern Sicily (southern Italy): Implications on Mount Etna volcanism. Tectonics 39, e2020TC006188.
Bassi, D., Bianchini, G., Mietto, P., Nebelsick, J.H., 2008. Southern Alps: Venetian Pre-Alps. In: McCann, T. (Ed.), The Geology of Central Europe, 2. The Geological Society London, pp. 1087–1092.
Beccaluva, L., Bonadiman, C., Coltorti, M., Salvini, L., Siena, F., 2001. Depletion events, nature of metasomatizing agent and timing of enrichment processes in lithospheric mantle xenoliths from the VVP. J. Petrol. 42, 173–187.
Beccaluva, L., Bianchini, G., Bonadiman, C., Coltorti, M., Milani, L., Salvini, L., Siena, F., Tassinari, R., 2007. Intraplate lithospheric and sublithospheric components in the Adriatic domain: nephelinite to tholeiite magma generation in the Paleogene Veneto Volcanic Province, Southern Alps. Special Paper of Geological Society of America 418, 131–152.
Beccaluva, L., Bianchini, G., Natali, C., Siena, F., 2011. Geodynamic control on orogenic and anorogenic magmatic phases in Sardinia and Southern Spain: Inferences for the Cenozoic evolution of the western Mediterranean. Lithos 123, 218–224.
Bellieni, G., Fioretti, A.M., Marzoli, A., Visonà, D., 2010. Permo–Paleogene magmtism inthe eastern Alps. Rendiconti Lincei, Scienze Fisiche e Naturali 21, 51–71.
Bergomi, M.A., Zanchetta, S., Tunesi, A., 2015. The Tertiary dike magmaism in the Southern Alps: geochronological data and geodynamic significance. Int. J. Earth Sci. 104, 449–473.
Bianchini, G., Bell, K., Vaccaro, C., 1999. Mantle sources of the Cenozoic Iblean volcanism (SE Sicily, Italy): Sr-Nd-Pb isotopic constraints. Mineral. Petrol. 67, 213–221.
Bianchini, G., Beccaluva, L., Siena, F., 2008. Post collisional and intraplate Cenozoic volcanism in the rifted Apennines/Adriatic domain. Lithos 101, 125–140.
Bianchini, G., Bryce, J.G., Blichert-Toft, J., Beccaluva, L., Natali, C., 2014. Mantle dynamics and secular variations beneath the East African Rift: Insights from peridotite xenoliths (Mega, Ethiopia). Chem. Geol. 386, 49–58.

Bracco Gartner, A.J.J., Seghedi, I., Nikogosian, I.K., Mason, P.R.D., 2020. Asthenosphere-induced melting of diverse source regions for East Carpathian post-collisional volcanism. Contrib. Mineral. Petrol. 175, 54.
Brack, P., 1984. Geologie der Intrusiva und Nebengesteine des Südwest–Adamello (Nord–Italien). Ph.D. thesis, Dissertation ETH. Nr. 7612.
Brombin, V., Bonadiman, C., Coltorti, M., Fahnestock, M.F., Bryce, J.G., Marzoli, A., 2018. Refertilized mantle keel below the Southern Alps domain (North–East Italy): evidence from Marosticano refractory mantle peridotites. Lithos 300–301, 72–85.
Brombin, V., Bonadiman, C., Jourdan, F., Roghi, G., Coltorti, M., Webb, L.E., Callegaro, S., Bellieni, G., De Vecchi, Gp, Sedea, R., Marzoli, A., 2019. Intraplate magmatism at a convergent plate boundary: the case of the Cenozoic northern Adria magmatism. Earth Sci. Rev. 192, 355–378.
Bryce, J.G., DePaolo, D.J., 2004. Pb isotopic heterogeneity in basaltic phenocrysts. Geochim. Cosmochim. Acta 68, 4453–4468.
Callegari, E., Brack, P., 2002. Geological map of the Tertiary Adamello batholith (Northern Italy). In: Explanatory notes and legend. Memorie di Scienze Geologiche, 54, pp. 19–49.
Castellarin, A., Vai, G.B., Cantelli, L., 2006. The Alpine evolution of the Southern Alps around the Giudicarie faults: a late cretaceous to early Eocene transfer zone. Tectonophysics 414, 203–223.
Cebriá, J.M., Wilson, M., 1995. Cenozoic mafic magmatism in Western/Central Europe: A common European asthenospheric reservoir? Terra Nova Abstracts 7, 162.
Conticelli, S., Guarnieri, L., Farinelli, A., Mattei, M., Avanzinelli, R., Bianchini, G., Boari, E., Tommasini, S., Tiepolo, M., Prelevic, D., Venturelli, G., 2009. Trace-elements and Sr–Nd–Pb isotopes of K–rich, shoshonitic, and calc-alkaline magmatism of the Western Mediterranean region: genesis of ultrapotassic to calcalkaline magmatic association in a post–collisional geodynamic setting. Lithos 107, 69–92.
Davies, J.H., von Blanckenburg, F., 1995. Slab breakoff: a model of lithosphere detachment and its test in the magmatism and deformation of collisional orogens. Earth Planet. Sci. Lett. 129, 85–102.
De Ritis, R., Pepe, F., Orecchio, B., Casalbore, D., Bosman, A., Chiappini, M., Chiocci, F., Corradino, M., Nicolich, R., Martorelli, E., Monaco, C., Presti, D., Totaro, C., 2019. Magmatism along lateral slab edges: insights from the Diamante-Enotrio-Ovidio volcanic-intrusive complex (Southern Tyrrhenian Sea). Tectonics 38, 2581–2605.
De Vecchi, G., Sedea, R., 1995. The Paleogene basalts of the Veneto region (NE Italy). Mem. Sci. Geol. 47, 253–374.
Dézes, P., Schmid, S.M., Ziegler, P.A., 2004. Evolution of the European Cenozoic Rift System: interaction of the Alpine and Pyrenean orogenes with their foreland lithosphere. Tectonophysics 389, 1–33.
Dilek, Y., Altunkaynak, S., 2009. Geochemical and temporal evolution of Cenozoic magmatism in Western Turkey: Mantle response to collision, slab break-off, and lithospheric tearing in an orogenic belt. Geol. Soc. Lond. Spec. Publ. 311, 213–233.
Eisele, J., Abouchami, W., Galer, S.J.G., Hofmann, A.W., 2003. The 320 kyr Pb isotope evolution of Mauna Kea lavas recorded in the HSDP-2 drill core. Geochem. Geophys. Geosyst. 4, 8710.
Faccenna, C., Funiciello, F., Civetta, L., D'Antonio, M., Moroni, M., Piromallo, C., 2007. Slab disruption, mantle circulation, and the opening of the Tyrrhenian basins. Geol. Soc. Am. Spec. Pap. 418, 153–169.
Ficini, E., Dal Zilio, L., Doglioni, C., Gerya, T.V., 2017. Horizontal mantle flow controls subduction dynamics. Sci. Rep. 7, 7550.
Funiciello, F., Faccenna, C., Giardini, D., 2004. Role of lateral mantle flow in the evolution of subduction systems: insights from laboratory experiments. Geophys. J. Int. 157, 1393–1406.
Gasperini, D., Bosch, D., Braga, R., Bondi, M., Macera, P., Morten, L., 2006. Ultramafic xenoliths from the Veneto Volcanic Province (Italy): Petrological and geochemical evidence for multiple metasomatism of the SE Alps mantle lithospere. Geochem. J. 40, 377–404.
Gvirtzman, Z., Nur, A., 1999. The formation of Mount Etna as the consequence of slab rollback. Nature 401, 782–785.
Handy, M.R., Schmid, S.M., Bousquet, R., Kissling, E., Bernoulli, D., 2010. Reconciling plate-tectonic reconstructions of Alpine Tethys with the geological–geophysical record of spreading and subduction in the Alps. Earth Sci. Rev. 102, 121–158.
Handy, M.R., Ustaszewki, K., Kissling, E., 2015. Reconstructing the Alps–Carpathians–Dinarides as a key to understanding switches in subduction polarity, slab gaps and surface motion. Int. J. Earth Sci. 104, 1–26.
Hart, S.R., 1984. A large-scale isotope anomaly in the Southern Hemisphere mantle. Nature 309, 753–757.
Hoernle, K., Zhang, Y.S., Graham, D., 1995. Seismic and geochemical evidence for largescale mantle upwelling beneath the eastern Atlantic and western and Central Europe. Nature 374, 34–39.
Hua, Y., Zhao, D., Xu, Y., 2017. P wave anisotropic tomography of the Alps. J. Geophys. Res. Solid Earth 122, 4509–4528.
Hürlimann, N., Müntener, O., Ulmer, P., Nandedkar, R., Chiaradia, M., Ovtcharova, M., 2016. Primary magmas in continental arcs and their differentiated products: petrology of a post-plutonic dyke suite in the Tertiary Adamello batholith (Alps). J. Petrol. 57, 495–534.
Irvine, T.N., Baragar, W.R.A., 1971. A guide to the chemical classification of the common volcanic rocks. Can. J. Earth Sci. 8, 523–548.
Ji, W.Q., Malusà, M.G., Tiepolo, M., Langone, A., Zhao, L., Wu, F.-Y., 2019. Synchronous Periadriatic magmatism in the Western and Central Alps in the absence of slab breakoff. Terra Nova 31, 120–128.
Kagami, H., Ulmer, P., Hansmann, W., Dietrich, V., Steiger, R.H., 1991. Nd–Sr isotopic and geochemical characteristics of the southern Adamello (Northern Italy) intrusives: implications for crustal versus mantle origin. J. Geophys. Res. Solid Earth 96, 14331–14346.
Kästle, E.D., Rosenberg, C., Boschi, L., Bellahsen, N., Meier, T., El-Sharkawy, A., 2020. Slab break-offs in the Alpine Subduction Zone. Int. J. Earth Sci. 109, 587–603.
Lapen, T.J., Johnson, C.M., Baumgartner, L.P., Dal Piaz, V., Skora, S., Beard, B.L., 2007. Coupling of oceanic and continental crust during Eocene eclogite-facies metamorphism: evidence from the Monte Rosa nappe, western Alps. Contrib. Mineral. Petrol. 153, 139–157.
LaTourette, T., Hervig, R.L., Holloway, J.R., 1995. Trace element partitioning between amphibole, phlogopite, and basanite melt. Earth Planet. Sci. Lett. 135, 13–30.
Le Maitre, R.W., Streckeisen, A., Zanettin, B., Le Bas, M.J., Bonin, B., Bateman, P., Bellieni, G., Dudek, A., Efremova, S., Keller, J., Lamere, J., Sabine, P.A., Schmid, R., Sorensen, H., Woolley, A.R., 2002. Igneous Rocks: A Classification and Glossary of Terms, Recommendations of the International Union of Geological Sciences Subcommission of the Systematics of Igneous Rocks. Cambridge University Press, UK.
Lee, J.Y., Marti, K., Severinghaus, J.P., Kawamura, K., Yoo, H.-S., Lee, J.B., Kim, J.S., 2006. A redetermination of the isotopic abundance of atmospheric Ar. Geochim. Cosmochim. Acta 70, 4507–4512.
Lustrino, M., Wilson, M., 2007. The circum-Mediterranean anorogenic Cenozoic igneous province. Earth Sci. Rev. 81, 1–65.
Macera, P., Gasperini, D., Piromallo, C., Blichert-Toft, J., Bosch, D., Del Moro, A., Martin, S., 2003. Geodynamic implications of deep mantle upwelling in the source of Tertiary volcanics from the Veneto region (Southern-Eastern Alps). J. Geodyn. 36, 563–590.
Macera, P., Gasperini, D., Ranalli, G., Mahatsente, R., 2008. Slab detachment and mantle plume upwelling in subduction zones: an example from the Italian South–Eastern Alps. J. Geodyn. 45, 32–48.
Malusà, M.G., Faccenna, C., Garzanti, E., Polino, R., 2011. Divergence in subduction zones and exhumation of high pressure rocks (Eocene Western Alps). Earth Planet. Sci. Lett. 310, 21–32.
Mats, V.D., Perepelova, T.I., 2011. A new perspective on evolution of the Baikal Rift. Geosci. Front. 2, 349–365.
McDonough, W.F., Sun, S.S., 1995. The composition of the Earth. Chem. Geol. 120, 223–253.
Medizza, F., 1965. Ricerche micropaleontologico-stratigrafiche sulle formazioni al limite tra Cretaceo e Terziario nell'alta Valle del Chiampo (Lessini Orientali). Mem. dell'Istituto Geol. Mineral. Univ. Padova 25, 1–41.
Merle, R., Marzoli, A., Aka, F.T., Chiaradia, J.M., Reisberg, L., Castorina, F., Jourdan, F., Renne, P.R., N'ni, J., Nyobe, J.B., 2017. Mt. Bambouto Volcano, Cameroon Line: mantle source and differentiation of within-plate alkaline rocks. J. Petrol. 58, 933–962.
Milani, L., Beccaluva, L., Coltorti, M., 1999. Petrogenesis and evolution of the Euganean magmatic complex, north eastern Italy. Eur. J. Mineral. 11, 379–399.
Moine, B.N., Grégoire, M., O'Reilly, S.Y., Sheppard, S.M.F., Cottin, J.Y., 2001. High field strenght elemental fractionation in the Upper Mantle: evidence from amphibole-rich composite mantle xenoliths from the Kerguelen Islands (Indian Ocean). J. Petrol. 11, 2145–2167.
Morten, L., Taylor, L.A., Durazzo, A., 1989. Spinel in harzburgite and lherzolite inclusions from the San Giovanni Ilarione Quarry, Lessini Mountains, Veneto Region, Italy. Mineral. Petrol. 40, 73–89.
Papazzoni, C.A., Giusberti, L., Carnevale, G., Roghi, G., Bassi, D., Zorzin, R., 2014. The Bolca Fossil-Lagerstätten: a window into the Eocene World. Rendiconti della Soc. Paleontol. Italiana 4.
Petrescu, L., Pondrelli, S., Salimbeni, S., Faccenda, M., AlpArray Working Group, 2020. Mantle flow below the central and greater Alpine region: insights from SKS anisotropy analysis at AlpArray and permanent stations. Solid Earth 11, 1275–1290.
Prelević, D., Akal, C., Romer, R.L., Mertz-Kraus, R., Helvaci, C., 2015. Magamtic response to slab tearing: constraints from the Afyon alkaline volcanic complex, Western Turkey. J. Petrol. 56, 527–562.
Roeder, P.L., Emslie, R.F., 1970. Olivine-liquid equilibrium. Contrib. Mineral. Petrol. 29, 275–289.
Rosenbaum, G., Lister, G.S., 2005. The Western Alps from the Jurassic to Oligocene: spatio-temporal constraints and evolutionary reconstructions. Earth Sci. Rev. 69, 281–306.
Rubatto, D., Hermann, J., 2001. Exhumation as fast as subduction? Geology 29, 3–6.
Rubatto, D., Gebauer, D., Fanning, M., 1998. Jurassic formation and Eocene subduction of the Zermatt-Saas-fee ophiolites: implications for the geodynamic evolution of the Central and Western Alps. Contrib. Mineral. Petrol. 132, 269–287.
Salimbeni, S., Malusà, M.G., Zhao, L., Guillot, S., Pondrelli, S., Margheriti, L., et al., 2018. Active and fossil mantle flows in the western Alpine region unravelled by seismic anisotropy analysis and high-resolution P wave tomography. Tectonophysics 731-732, 35–47.
Schaltegger, U., Nowak, A., Ulianov, A., Fiscer, C.M., Gerdes, A., Spikings, R., Whitehouse, M.J., Bindeman, I., Hanchar, J.M., Duff, J., Vervoort, J.D., Sheldrake, T., Caricchi, L., Brack, P., Müntener, O., 2019. Zircon petrochronology and $^{40}Ar/^{39}Ar$ thermochronology of the Adamello Intrusive Suite, N. Italy: monitoring the growth and decay of an incrementally assembled magmatic system. J. Petrol. 60, 701–722.
Siena, F., Coltorti, M., 1989. Lithospheric mantle evolution: evidences from ultramafic xenoliths in the Lessinean volcanics (Northern Itlay). Chem. Geol. 77, 347–364.
Siena, F., Coltorti, M., 1993. Thermobarometric evolution and metasomatic processes of upper mantle in different tectonic settings: evidence from spinel peridotite xenoliths. Eur. J. Mineral. 5, 1073–1090.
Stampfli, G.M., Mosar, J., Marquer, D., Marchant, R., Baudin, T., Borel, G., 1998. Subduction and obduction processes in the Swiss Alps. Tectonophysics 296, 159–204.

Stampfli, G.M., Borel, G.D., Marchant, R., Mosar, J., 2002. Western Alps geological constraints on western Tethyan reconstruction. In: Rosenbaum, G., Lister, G.S. (Eds.), Reconstruction of the Evolution of the Alpine-Himalayan Orogen. Journal of the Virtual Explorer, vol. 7, pp. 75–104.

Sun, S.S., McDonough, W.F., 1989. Chemical and isotopic systematics of oceanic basalts: Implications for mantle composition and processes. In: Saunders, A.D., Norry, M.J. (Eds.), Magmatism in the Oceanic Basins, vol. 42. Geological Society, London, Special Publications, pp. 313–346.

Svensen, H.H., Torsvik, T.H., Callegaro, S., Augland, L., Heimdal, T.H., Jerram, D.A., Planke, S., Pereira, E., 2018. Gondwana Large Igneous Provinces: plate reconstructions,volcanic basins and sill volumes. Geol. Soc. Lond., Spec. Publ. 463, 17–40.

Visonà, D., Caironi, V., Carraro, A., Dallai, L., Fioretti, A.M., Fanning, M., 2007. Zircon megacrysts from basalts of the venetian Volcanic Province (NE Italy): U–Pb, oxygen isotopes and REE data. Lithos 94, 168–180.

Wiederkehr, M., Sudo, M., Bousquet, R., Berger, A., Schmid, S.M., 2009. Alpine orogenic evolution from subduction to collisional thermal overprint: the $^{40}Ar/^{39}Ar$ age constraints from the Valaisan Ocean, Central Alps. Tectonics 48, TC6009.

Wilson, M., Bianchini, G., 1999. Tertiary-Quaternary magmatism within the Mediterranean and surrounding regions. Geol. Soc. Lond., Spec. Publ. 156, 141–168.

Wilson, M., Downes, H., 2006. Tertiary-Quaternary intra-plate magmatism in Europe and its relationship to mantle dynamics. In: Gee, D., Stephenson, R. (Eds.), European Lithosphere Dynamics, vol. 32. Geological Society, London, Memoirs, pp. 147–166.

Zhao, L., Paul, A., Malusà, M.G., Xu, X., Zheng, T., Solarino, S., Guillot, S., Schwartz, S., Dumont, T., Salimbeni, S., Aubert, C., Pondrelli, S., Wang, Q., Zhu, R., 2016. Continuity of the Alpine slab unraveled by high-resolution P wave tomography. J. Geophys. Res. Solid Earth 121, 8720–8737.

Zindler, A., Hart, S., 1986. Chemical geodynamics. Annu. Rev. Earth Planet. Sci. 14, 493–571.